Dynamic Observation of Solidification and Solidification Cracking during Welding with Optical Microscope (I)†

— Solidification Front and Behavior of Cracking —

Fukuhisa MATSUDA*, Hiroji NAKAGAWA**and Kazuhiko SORADA***

Abstract

Dynamic behaviors of solidification front and solidification cracking during welding of different steels have been observed with high speed cinecamera mounted on optical microscope. The dynamic observation of the solidification front has revealed very narrow apparent solidification temperature range compared with true solidification temperature range. The dynamic observation of the solidification cracking in rapid tensile test has revealed that crack initiation occurs at high temperature part in true solidification temperature range and that the crack propagates toward both higher and lower temperature regions. These observations have been well explained from the viewpoint of solidification theory. Moreover, a new concept of solidification cracking has been proposed on the basis of these observations.

KEY WORDS: (Solidification) (Hot Cracking) (Carbon Steels) (Stainless Steels) (Nickel Alloys)

1. Introduction

In fusion welding solidification phenomena directly or indirectly influence formation of defects, mechanical and mechanochemical properties of weld metal. Thus full explication of solidification mechanism and desired control of solidification behavior are very important subject for development of fusion welding.

Solidification theories including the concept of "Constitutional Supercooling" and experimental studies have been well developed for this about thirty years[1], and simultaneously solidification structure of weld metal have been explained by the concept of constitutional supercooling combining the peculiarities in welding[2)-5)].

These studies, however, are yet difficult to throw light upon fresh or live solidification behavior as it is, because most of studies have been done on the microstructure after solidification except for the direct observation on organic materials.

Likewise, mechanism of weld solidification cracking has been studied and proposed by many researchers so far[6], but some inevitable speculations and hypothesis have been included in the proposed mechanism, because they also have been based on the observation of solidification microstructure and the crack at room temperature after welding.

On the other hand, in-situ or direct observation technique of solidification front during TIG-arc welding with optical microscope has been developed by some investigators[7)-12)], and interesting dynamic movement of solidification front has been revealed. Certainly, TIG-arc welding is superior to casting in in-situ observation, because molten and solidifying metal is directly visible under inert gas shielding. Therefore systematic and analytic study on direct obeservation on the basis of solidification theory and establishing the relation between solidification phenomena and solidification cracking have been important subject.

Therefore the authors have tried to directly observe and analyze the solidification front and solidification cracking behavior of plain carbon steels of different carbon contents, several stainless steels and an Inconel alloy. This trial has brought very interesting discover and understanding of solidification and solidification cracking behavior, and moreover has yielded a new concept of solidification cracking.

2. Materials Used and Experimental Procedures

2.1 Materials Used

Materials used were 9 kinds of plain carbon steels

† Received on September 30, 1982

* Professor

** Research Instructor

*** Graduate Student of Osaka Univ., now with Sumitomo Heavy Industries, LTD.

Transactions of JWRI is published by Welding Research Institute of Osaka University, Ibaraki, Osaka, Japan

Table 1 Chemical compositions of materials used

Materials	Composition (wt.%)							
	C	Si	Mn	P	S	Ni	Cr	Others
SPHC(1)	<0.05	<0.01	0.30	0.017	0.020	-	-	-
SPHC(2)	0.05	0.19	0.30	0.043	0.013	-	-	-
SPHT(1)	0.07	0.01	0.34	0.008	0.008	-	-	-
SPHT(2)	0.10	0.01	0.45	0.011	0.013	-	-	-
SM50B	0.15	0.45	1.29	0.018	0.015	-	-	-
S15C	0.17	0.01	0.59	0.010	0.013	-	-	-
S35C	0.34	0.02	0.77	0.023	0.017	-	-	-
S55C	0.52	0.23	0.67	0.017	0.033	-	-	-
SK6	0.77	0.22	0.43	0.020	0.009	-	-	-
Fe-2%Ni	<0.05	0.01	<0.01	0.003	0.006	1.95	-	-
Fe-5%Ni	<0.05	<0.01	<0.01	0.003	0.006	5.06	-	-
Fe-7%Ni	<0.05	<0.01	<0.01	0.003	0.006	7.41	-	-
SUS304	0.05	0.54	0.54	0.028	0.005	8.53	18.08	-
SUS310S	0.05	0.60	0.60	0.023	0.005	19.03	25.33	-
SUS430	0.07	0.44	0.39	0.022	0.007	0.09	16.06	-
Inconel 600	0.10	0.10	0.16	0.008	<0.005	75.56	15.64	Fe:7.34, Cu:0.32

containing 0.05 to 0.77% carbon, Fe-2, 5 and 7% Ni binary alloys, and Inconel alloy 600. All the materials were commercial ones except for the Fe-Ni alloys made by tentative vacuum melting. Their chemical compositions are shown in **Table 1**, where designations for the commercial materials except for the Inconel alloy follow Japan Industrial Standard (JIS). Their thickness was 2 mm except for SUS430 of 1.5mm.

2.2 Equipment and Procedure for Observation of Solidification Front

Arrangement of equipment and specimen is illustrated in **Fig. 1**, which was composed of a TIG torch, a specially designed trailer shielding nozzle with a glass window on the top, an optical microscope with large working distance of 87mm, a back shielding device of Ar gas, an illumination system improving image contrast, and a carriage of specimen. High speed 16mm cinecamera or 35mm motor driving camera was mounted on the microscope. The microscope has zooming mechanism from x0.66 to x4 in objection lens. For the purpose of the observation of solidification front the zooming was set to x4, and eyepiece lens of x10 or x20 was combined.

During welding the TIG torch and the microscope were fixed, and the specimen was moved with the carriage. The specimen was 100mm square. Welding conditions generally used were; welding current of 70 to 75A, arc voltage of 14 to 16V, and welding speed of 40mm/min, which made weld bead of about 8mm in width on both top and back surfaces. Thus the heat flow along thickness direction is negligible.

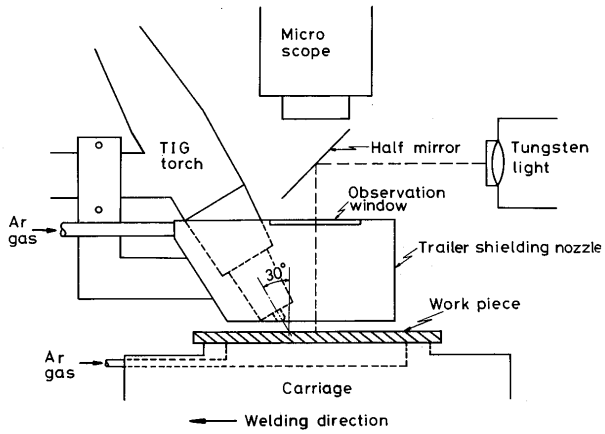

Fig. 1 Equipment for dynamic observation of solidification front during TIG-arc welding

2.3 Equipment and Procedure for Observation of Solidification Cracking

The equipment shown in Fig. 1 was coupled to a universal tensile cracking tester whose tensile speed can be widely varied with a motor. Specimen configuration is shown in **Fig. 2**, which has two holes for pins of chuck and notches to concentrate applying displacement to welded zone.

Welding conditions were; welding current of 75 to 80A, arc voltage of 14 to 16V, welding speed of 50mm/min, which made weld bead of 7 to 8 mm in width on both top and back surfaces. When the TIG torch passed near the middle point of weld length, the specimen was rapidly pulled perpendicularly to the weld line. Just before the pulling, the high speed cinecamera was started at 400 frames/sec, when the zooming was set to xl and eyepiece lens of x10 was combined. The tensile speed was set to 10mm/sec

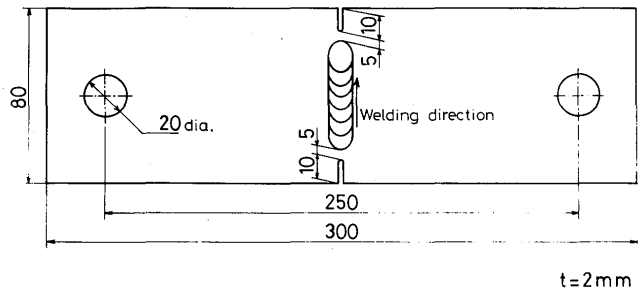

Fig. 2 Specimen configuration for dynamic observation of solidification cracking

which is the maximum speed of this tester in order to clearly reveal the relation between the temperature in weld metal and the position of initiation and propagation of solidification crack. The temperature in weld metal was measured in a different specimen with W/5%Re-W/26%Re thermocouple of 0.3mm dia.

The cine-film after development was analyzed with a film motion analyzer in magnification of about x40 to measure the crack initiation point and propagating characteristics vs. the lapse of time.

3. Experimental Results and Discussion

3.1 Characteristics of Solidification Front

As the best example of direct observation, the solidification fronts of Inconel alloy 600 are shown in **Fig. 3.** Cellular dendritic substructure and grain boundaries between columnar grains are clearly observed, and secondary dendrite arms also can be observed in Fig. 3(b) which was welded with specially high heat input (70A, 14 to 16V, and 10mm/min). Interestingly some tips of cellular dendrites extend a little into the molten puddle in both (a) and (b).

By means of this observation solid-liquid coexistent zone, namely solidification range can be measured, which is of course an apparent zone dependent on the dissolving power of the microscope used. In Fig. 3(a) the apparent solid-liquid coexistent zone is 300 to 400 μm, and this corresponds to about 30 to 40°C of solidification temperature range.

The solidification front of fully austenitic stainless steel SUS310S is shown in **Fig. 4,** where celluar or cellular dendritic substructure is clearly seen. The apparent solidification temperature range was also about 30 to 40°C. It should be noticed, however, that substructure-like patterns are also seen extremely near the solidification front, the size of which is several times larger than true substructure. Depending on material and welding conditions, such substructure-like patterns dominated the solid-liquid coexistent zone instead of the true substructure and remained

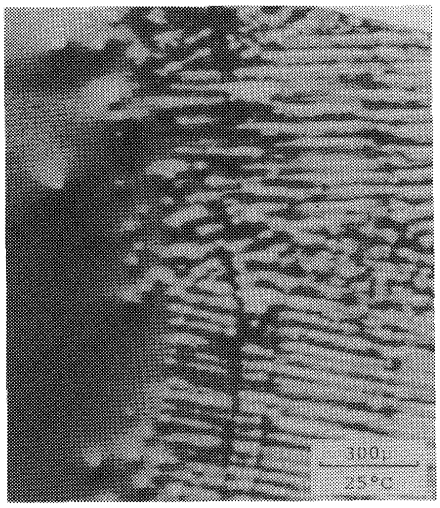

(a) Standard heat input

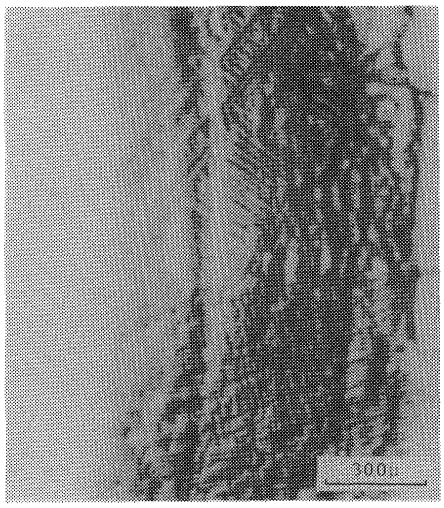

(b) higher heat input than (a)

Fig. 3 Solidification front of Inconel alloy 600

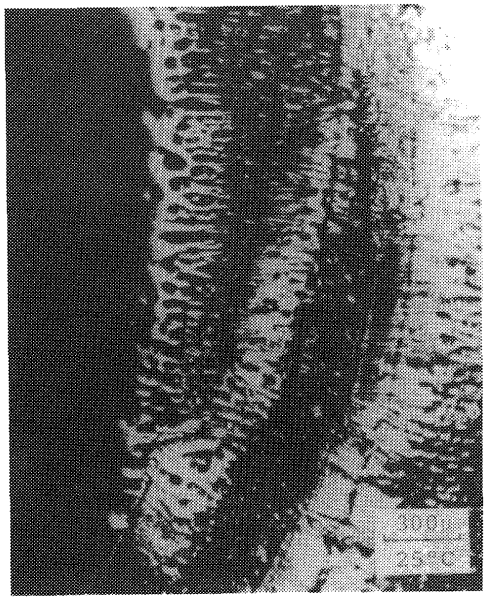

Fig. 4 Solidification front of fully austenitic stainless steel SUS310S

Fig. 5 Substructure-like pattern remaining at room temperature in SUS304 (120A, 15V, 130mm/min)

at room temperature as shown in **Fig. 5.** Generally higher the welding speed was, the more the substructure-like patterns were dominant. It is considered that the pattern is related to surface tension and/or viscosity of liquid metal depending on composition and temperature distribution. In spite of such false pattern, however, it was possible to measure the apparent solid-liquid coexistent zone.

Then, **Fig. 6** shows solidification fronts of plain carbon steels of different carbon contents. In carbon content less than about 0.10% the solidification front is appoximately planar, although small triangular patterns are often observed in 0.07% carbon, which are phenomena peculiar to surface only and maybe caused by local dendritic chase in order to make up leeway of solidification due to minute gas bubbling judging from the dynamic observation with high speed cinecamera during welding and its magnified feature after welding with scanning electron microscope as shown in **Fig. 7.** Such triangular patterns were observed more or less in other materials. In carbon content more than about 0.10% the indentations of solidification front were clearly seen and became more

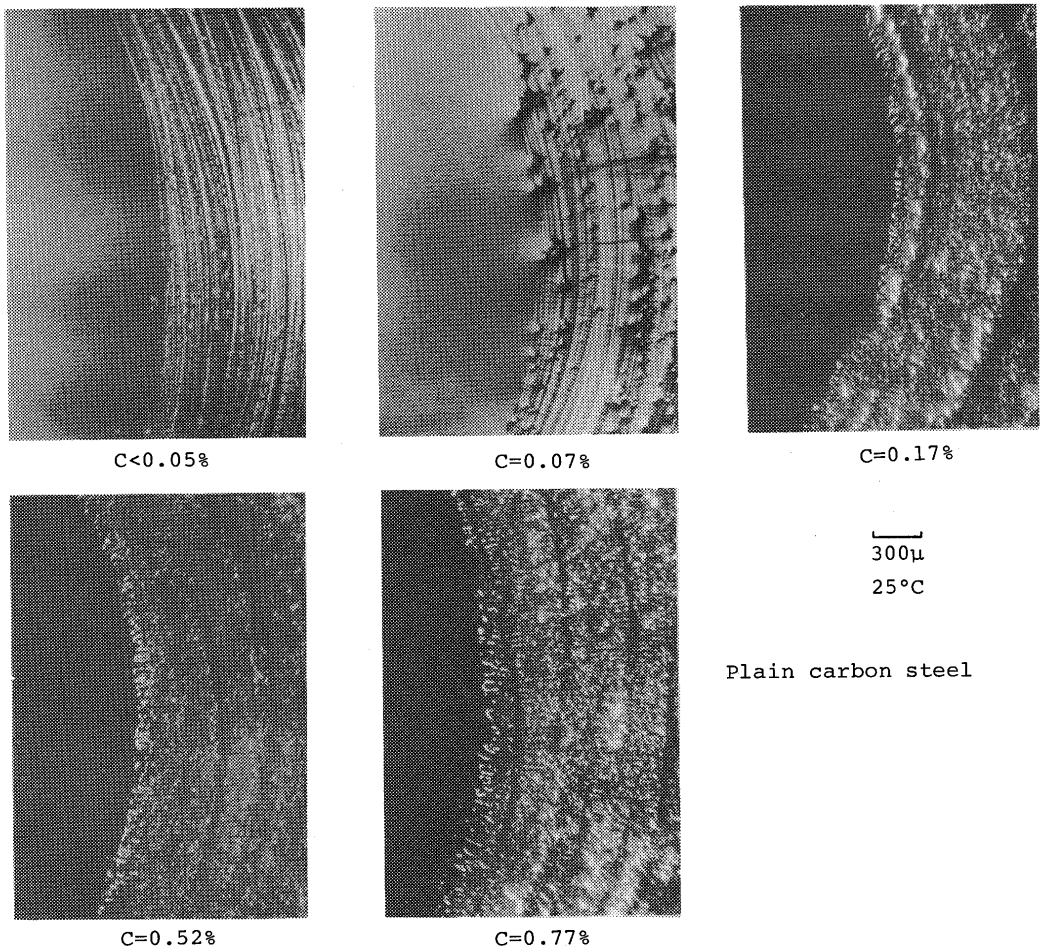

Fig. 6 Solidification fronts of plain carbon steels

and more conspicuous together with the carbon content. In other words, the apparent solid-liquid coexistent zone increased together with the carbon content. Their corresponding solidification temperature ranges were about 10°C in 0.17% carbon, about 20°C in 0.34% carbon and about 30 to 40°C in 0.77% carbon.

Although peritectic reaction must have occurred in the range of carbon content between 0.10% and 0.50% judging from Fe-C phase diagram, no peculiar phenomenon was observed near solidification front.

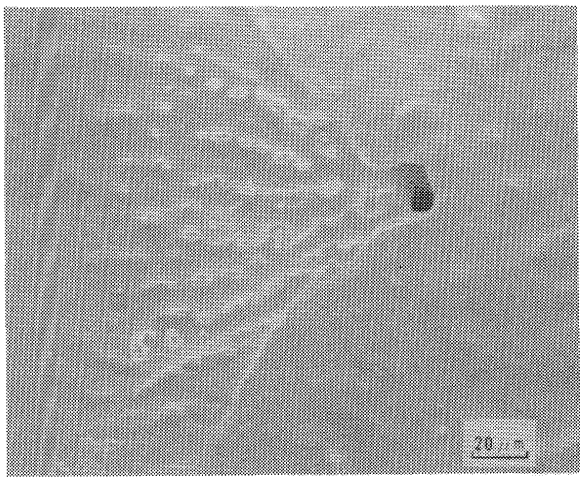

Fig. 7 SEM observation of triangular pattern peculiar to bead surface in SPHT(2)

Also in Fe-Ni binary alloys, no peculiar phenomenon due to peritectic reaction was observed in Fe-5% Ni alloy.

The solidification front of austenitic stainless steel SUS304 was similar to that of fully austenitic stainless steel SUS310S already shown in Fig. 4, although peritectic and/or eutectic reaction of δ and γ occur during solidification of SUS304[13),14)]. The solidification front of SUS430 was similar to that of high carbon steel.

As a whole, it is worth notice that the apparent solid-liquid coexistent zone or the solidification temperature range observed by the direct observation is narrow unexpectedly.

3.2 Characteristics of Initiation and Propagation of Solidification Cracking

An example of sequence of high speed cine-film photographing the cracking behavior at the rapid pulling of fully austenitic stainless steel SUS310S is shown in **Fig. 8.** At a short lapse after the start of pulling the initiation of solidification crack occurred at about 0.5mm behind the solidification front as shown in (a), when the time is defined to be 0 msec in Fig. 8. Then, the crack propagated to both lower and higher temperature zones, and the crack in the higher temperature zone almost reached the solidification

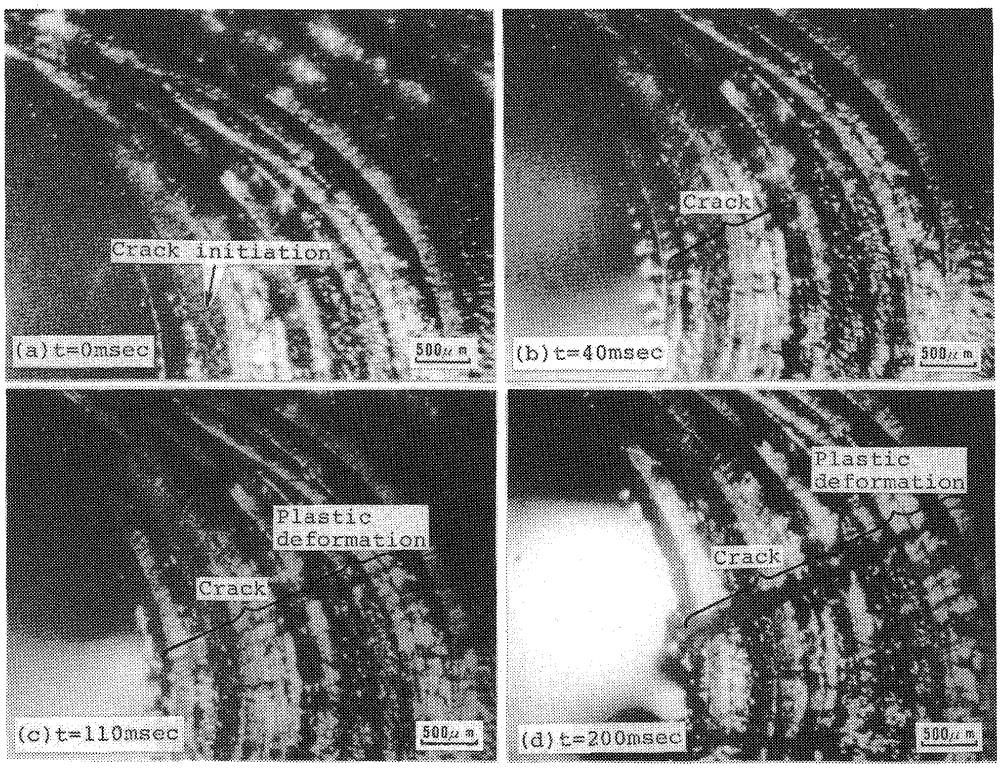

Fig. 8 An example of sequence of cine-films during cracking test of SUS310S

front at 40msec in (b). The crack in the lower temperature zone further developed and stopped at 110msec in (c). After that the crack developed no longer, but only crack width increased as seen in (d).

The relation between time after the crack initiation and positions of the both crack tips in the lower and the higher temperature zones in Fig. 8 is shown in **Fig. 9.** The same relations in plain carbon steels are shown in **Fig. 10.** In Figs. 9 and 10 the crack length increases with the time and gradually reaches a finite value, namely the maximum crack length L_{max}. This L_{max} can be converted into brittleness temperature range BTR[15]. Now it is very noteworthy that the crack initiation point locates at about one third of L_{max}. That is to say, the crack initiation temperature locates at about one third of BTR, or in more generous expression at relatively high temperature part. The similar behavior of crack initiation was observed in the Trans-Varestraint testing by one of the authors[16]. Such phenomenon is contrary to the concept that the crack initiation should occur at a lower temperature zone in BTR according to the conventional theory like "Generalized Theory"[6].

Also it is noticed that the initial propagating speed of the crack measured as the slope in Figs. 9 and 10 is generally somewhat slower in the higher temperature zone of the initiation point than that in the lower temperature zone. One of the reason of this is considerd to be "healing", because clear evidence of inflow of liquid metal into crack just after the increment of the width of crack was sometimes caught in high speed cine-film.

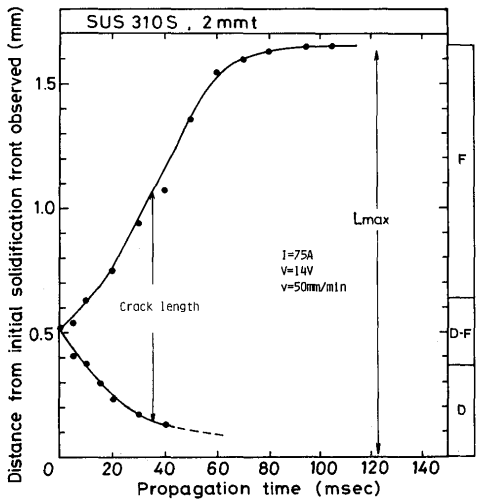

Fig. 9 Relation between time after crack initiation and positions of crack tips during cracking test of SUS310S

3.3 Discussion

3.3.1 Evaluation of true solidification temperature range

It is difficult to measure or evaluate the true solidus temperature at which remaining little liquid enriched with impurities solidifies completely. The authors[17] have shown in a fractographic study on weld solidification crack of fully austenitic stainless steel SUS310S made with the Trans-Varestraint testing that the feature of the crack surface gives the distribution and the state of the remaining liquid during solidification, and that the lower limit temperature of BTR reasonably corresponds to the true solidus temperature. That is to say, BTR reasonably corresponds to true solidification temperature range.

Now, on this viewpoint **Table 2** compares the data in this study with one another, namely the apparent solidification temperature range ΔT_a measured by

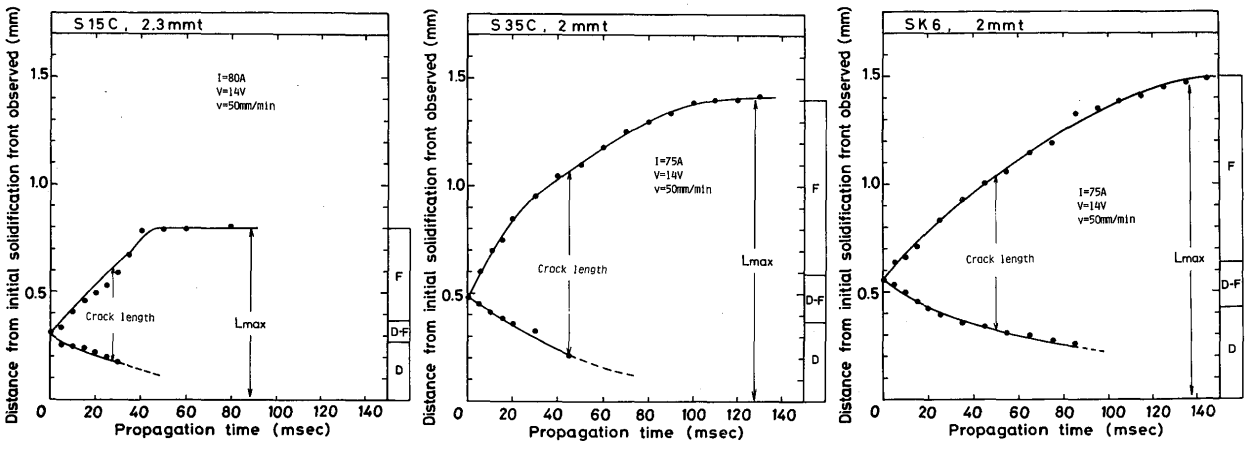

(a) S15C (b) S35C (c) SK6

Fig. 10 Relation between time after crack initiation and positions of crack tips during cracking test

Table 2 Comparison among apparent solidification range ΔT_a, nominal solidification range ΔT_n, temperature difference between liquidus and crack initiation point ΔT_{L-C}, and true solidification range ΔT_{BTR}.

Material	ΔTn* (°C)	ΔTa (°C)	ΔT_{L-C} (°C)	ΔT_{BTR} (°C)
S15C	-	10	20	65
S35C	-	20	30	100
SK6	-	30-40	40	130
SUS310S	55	30-40	40	150
Inconel 600	-	30-40	-	120

*Metals Handbook, 8th edition, Vol. 1. 1961.

the dynamic observation, nominal solidification temperature range ΔT_n, the temperature difference between the liquidus and the crack initiation point ΔT_{L-C} and the true solidification temperature range measured as the brittleness temperature range ΔT_{BTR}. It is understood that $\Delta T_a/\Delta T_{BTR}$ is less than about 0.2 or 0.3, and that ΔT_{L-C} is nearly equal with or slightly larger than ΔT_a. The latter means that the crack initiation occurred near or just behind the apparent solidus temperature.

These suggest that neighbouring cellular dendrites rapidly develop to contact with each other in an early stage of solidification below the liquidus temperature, and thus so called "liquid film stage" responsible to solidification crack already occurs in an early stage near liquidus temperature.

3.3.2 *Fractographic feature*

As already mentioned, the fractographic feature of solidification crack gives important information as regards solidification phenomena. The authors[17] have also shown that the crack surface of SUS310S made with the Trans-Varestraint testing has three different regions of Types D, D-F and F. Type D has a dendritic feature, Type F has a flat feature and Type D-F has a transient feature from D to F. Precisely describing, Type F has a flat feature with many small voids paralleling with growth direction of columnar crystal. There are inclusions in these voids which were identified as remaining liquid droplets at the cracking moment. Morerver, the ductility in Type F gradually increases in the decreasing direction of temperature. Therefore it was imagined[17] that the remaining liquid in Type F is not already so much as to fully cover the grain boundary, but is dispersed and becomes more and more sporadic with the decrease in temperature. In other words, Type F is not so called liquid film stage, but liquid lake or liquid droplet stage because of the dispersed remaining liquids. Therefore it is considerd that Type D-F is the liquid film stage. Furthermore, in aluminum alloys bulk solidus temperature measured by usual thermal analysis in electric furnace well locates at the temperature region of Type D-F in the Trans-Varestraint testing[18].

Now, **Fig. 11** shows fractographs of solidification cracks of S35C and SUS310S in this study. They also have Types D, D-F and F regions. It is noteworthy that the crack initiation point locates on Type D-F. (See also the right ordinate in Figs. 9 and 10.)

From these circumstantial evidences it can be estimated that the initiation of solidification crack occurs at the liquid film stage which is in a relatively high temperature part in the true solidification temperature range.

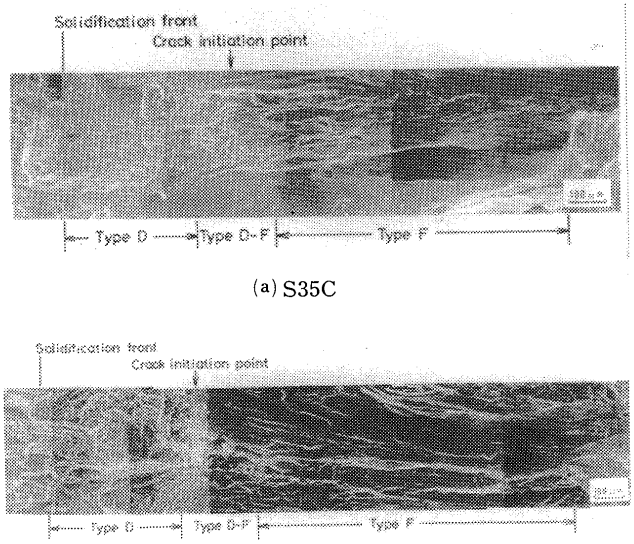

(a) S35C

(b) SUS310S

Fig. 11 SEM fractographs of solidification cracks

3.3.3 *Theoretical approach*

Such rapid developing characteristics of cellular dendrites and thus early attainment of liquid film stage can be well recognized by the next rough theoretical estimation. Solute content of remaining liquid during solidification, when the content is uniform in the liquid, is approximately given by the next modified Scheil's equation[19].

$$C_l = C_o \{1 - (1 - 2\alpha k) f_s\}^{k-1/1-2\alpha k} \quad (1)$$

where

C_l = solute content in the liquid when the solid fraction within a closed "volume element" is f_s;

C_o = initial solute content;

k = equilibrium distribution coefficient;

$\alpha = D_s \cdot t_f/L^2$ (D_s: diffusion coefficient of solute in

solid, t_f: local solidification time, L: growth length in the volume element (generally one half of dendrite arm spacing))

When $\alpha = 0$, namely the diffusion in solid is negligible, Eq. (1) becomes classical Scheil's equation. When $\alpha = 0.5$, Eq. (1) gives the relation between C_l vs. f_s in equilibrium solidification. Refer to reference 20) as regards the propriety of the assumption that the solute content in liquid is generally uniform during weld solidification.

On the other hand, the relation between C_l and liquidus temperature T_l for C_l is approximately given by the next equation.

$$T_l = T_o - m\,(C_l - C_o) \tag{2}$$

where

T_o = liquidus temperature at C_o;

m = slope of liquidus line in phase diagram.

Combining Eqs. (1) and (2), next equation giving the relation between temperature drop from initial liquidus temperature and solid fraction is obtained.

$$\Delta T \equiv T_o - T_l = mC_o\left[\{1-(1-2\alpha k)f_s\}^{k-1/1-2\alpha k}-1\right] \tag{3}$$

Ep. (3) can be extended to Eq. (3') for the system containing n kinds of solute elements under the assumption that liquidus surface is plane.

$$\Delta T = \sum_{i=1}^{n} m_i C_{io}\left[\{1-(1-2\alpha_i k_i)f_s\}^{k_i-1/1-2\alpha_i k_i}-1\right] \tag{3'}$$

The relations between temperature and solid fraction in three plain carbon steels and fully austenitic stainless steel are show in **Figs. 12** and **13** respectively. The plain carbon steels are assumed to be Fe-C binary alloys, and calculation was done for two conditions of no diffusion and complete diffusion in solid. Actual relation must exist near the curve of complete diffusion because of the high diffusivity of carbon. The fully austenitic stainless steel is assumed to be Fe-C-Si-Mn-P-S-Cr-Ni plural alloy, and calculation was done in the condition of complete diffusion of carbon and no diffusion of the other elements in solid, referring Fe-Cr-Ni phase diagram[21], other Fe-binary phase diagram[22),23)] and distribution coefficient in Fe-Cr-Ni alloys[24)]

It is noticeable in Figs. 12 and 13 that the solid fraction more than 0.6 is attained at temperature drop of mere about 20°C from the initial liquidus except for the fraction of 0.4 in SK6. This means rapid development of solid in an early stage of solidification.

On the other hand it has been shown in aluminum alloy casting[25),26)] that the solid fraction at which

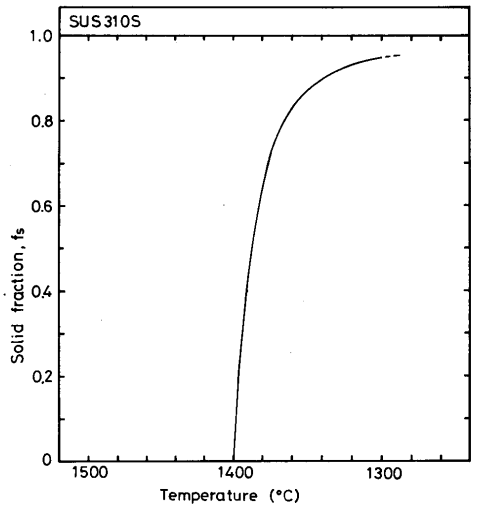

Fig. 13 Calculated relation between temperature and solid fraction during solidification of SUS310S

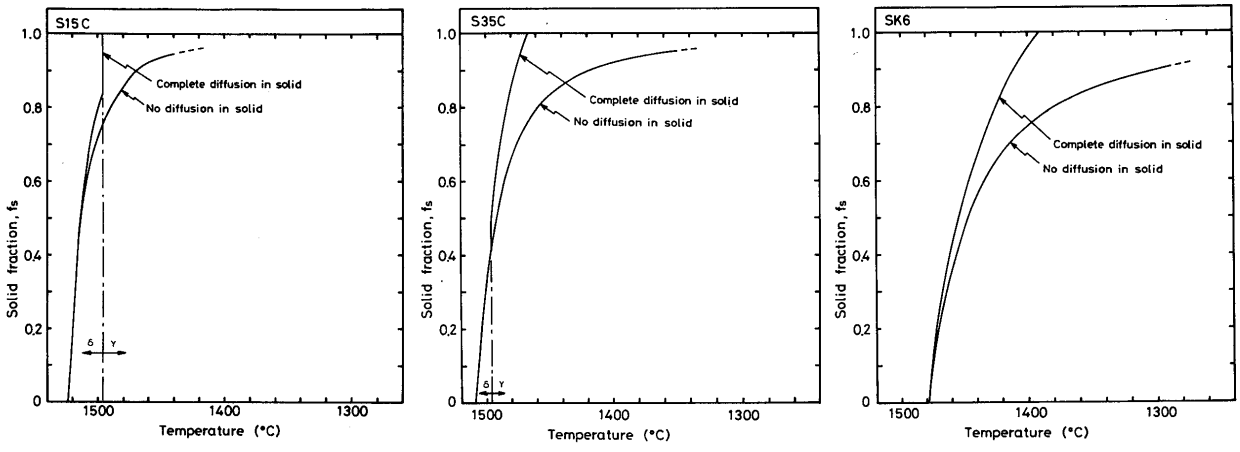

(a) S15C (b) S35C (c) SK6

Fig. 12 Calculated relation between temperature and solid fraction during solidification

dendrites begin to form networks is 0.31, and that the solid fraction above which the interdendritic liquid cannot flow is 0.67, and that strength during solidification originates at 0.67. Moreover it has been shown[27] by rheological study that specimens containing more than about 0.15 solid fraction exhibit apparent yield point. Comparison of Figs. 12 and 13 with Table 2 shows that the solid fraction of the crack initiation point is about 0.6 to 0.8. Of course the values in these references and in Figs. 12 and 13 give only mean solid fraction of dendritic growth, and thus it must be imagined that the tip of secondary dendrite arm grows far away from the mean value and that the valley between the arms doesn't reach the mean value. Such a predominant growth of secondary dendrite during an early stage of solidification has been experimentally confirmed with isothermal-transformation technique[28]. Therefore the previous studies referred and present experimental and calculated results consistently support the rapid developing characteristic of cellular dendrites in an early stage of solidification and thus early attainment of liquid film stage. Now it must be emphasized that the term "liquid film stage" in this study doesn't mean the state where the solid is fully covered with thin liquid, because dendrites already form networks according to reference 25) and 26) and judging from the direct observation in this study. Thus it may be imagined that in liquid film stage there are remaining thin liquids of small dihedral angle at grain boundary which is just formed by the networks of dendrites.

4. Proposal of New Concept of Solidification Cracking

Borland's "Generalized Theory" has been generally well accepted as the concept of solidification cracking and its mechanism, of which one of the major foundation is illustrated in **Fig. 14.** In stage 1, the solid phase is dispersed while the liquid is continuous. In stage 2, both liquid and solid phase are continuous, but only the liquid is capable of movement for "healing". In stage 3, the semi-continuous network of the solid phase restricts the free passage of liquid. Stage 3 is called the "critical solidification range", because cracking occurs late in the solidification cycle in a critical solidification range where fissures that are developed are no able to be healed because the advanced development of the grains prevents the free passage of liquid[29]. This concept was based on the idea that the solid phase gradually advances with the temperature drop as seen in Pellini's model[30]. As

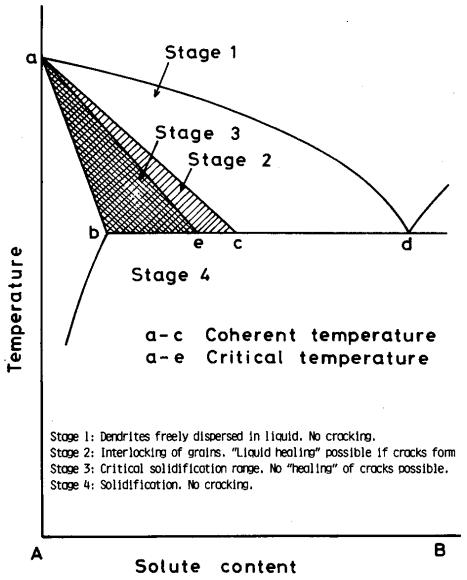

Fig. 14 Concept of cracking susceptibility on phase diagram in Generalized Theory[6]

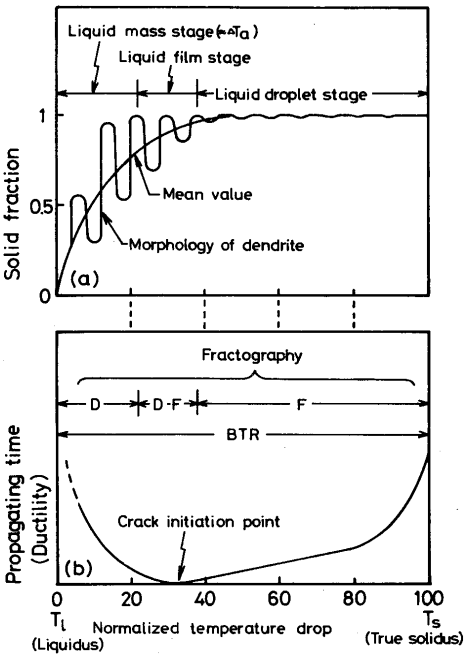

Fig. 15 A new concept of cracking susceptibility during solidification

shown in this study, however, the solid phase rapidly advances in an early stage of solidification.

Therefore the authors would like to propose a new concept of solidification cracking as shown in **Fig. 15,** where some variables of solidification and solidification cracking are represented in relation to normalized temperature drop between liquidus T_l and true solidus T_s. At first (a) shows the rapid growth mode of secondary dendrite in an early stage of solidification and the resultant distribution of remaining liquid. It must be noticed that so called "liquid film stage"

occurs in an early stage of solidification and thus the subsequent long period is so to speak "liquid droplet stage" because of the dispersed remaining liquids. The earliest stage is named "liquid mass stage". Of course such terminologies are not strict, and only used to easily catch the image of the remaining liquid. It must be emphasized that the liquid film stage doesn't mean the state where the solid is fully covered with thin liquid. In this proposal dendrites already form networks in the liquid film stage. Coherent temperature[6] by Borland locates at latter part in the liquid mass stage, and the critical temperature[6] is the boundary between the liquid mass and the liquid film stage. Then (b) gives the characteristics of initiation and propagation of solidification cracking in this study and the fractographic features. Solidification crack occurs at the liquid film stage and propagates toward both the liquid mass and the liquid droplet stages. The propagating speed in the liquid mass stage is generally somewhat slower than that in the high temperature zone of the liquid droplet stage because of "healing".

This new concept improves one of the foundation of "Generalized Theory" as shown in **Fig. 16.** Stages 1 and 2 are shifted to the zone extremely near the liquidus temperature. Now stage 3 is divided into stage 3(h) and stage 3(l), because the stage 3(h) is susceptible to crack initiation due to the liquid film stage, and the stage 3(l) is susceptible not to crack initiation but to propagation due to the liquid droplet stage.

In applying this concept, the following should be considered: In most case of practical welding, deformation causing the formation of solidification crack continues longer than the instantaneous deformation in this study. In this practical case, the crack once formed will surely propagate at the most susceptible stage, namely at the liquid film stage or the stage 3(h) to follow the movement of heat source. This is the reason why the fractographs of solidification crack in most case show some dendritic feature[31)-33)] and why the flat feature (Type F) corresponding to the liquid droplet stage is observed only at the location where the crack was arrested[32)].

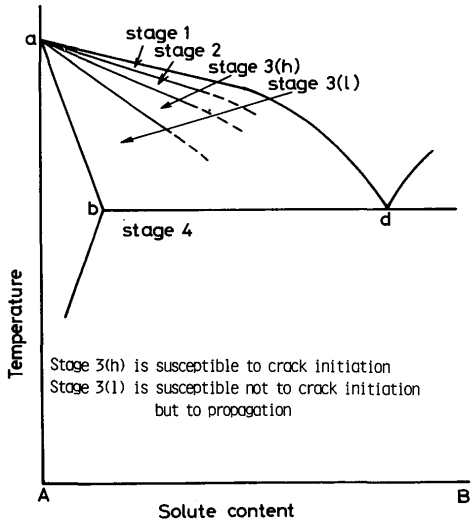

Fig. 16 Improved concept of cracking susceptibillty on phase diagram

5. Conclusion

Direct observation of solidification phenomena and solidification cracking in plain carbon steels, several stainless steels and an Inconel alloy during welding was done and analyzed by solidification theory, and a new concept of solidification cracking was proposed.

Main conclusions obtained are as follows:

1) Apparent solidification temperature range observed with microscope is very narrow compared with the true solidification temperature range measured as the brittleness temperature range. In plain carbon steel the apparent solidification temperature range is increased with the carbon content from nearly nil in carbon content less than 0.10% up to about 30 to 40°C in carbon content of about 0.8%. In stainless steels and Inconel alloy the range is about 30 to 40°C.

2) The concluson 1) can be related with rapid developing characteristic of cellular dendrites, and is well understood from the viewpoint of solidification theory.

3) Solidification crack in rapid tensile cracking test occurs at high temperature part in the true solidification temperature range and propagates toward both higher and lower temperature region.

4) The conclusion 3) and fractographic study revealed that so called liquid film stage is attained in an early stage of true solidification temperature range.

5) Combining conclusions 1) to 4), a new concept of solidification cracking was proposed, where the initiation and the propagation characteristics of solidification crack are related to the situation of remaining interdendritic liquid. The most peculiar feature of this new concept is shifting of the crack susceptible region to the high temperature zone near liquidus contrary to the conventional concept.

Acknowledgement

The authors would like to thank Mitsubishi Heavy Ind. for the offering of materials.

References

1) B. Chalmers: "Principles of Solidification", John Wiley & Sons, 1964, p.152.
2) W.F.Savage, etal: Weld. J., Vol. 44(1965), 175s.
3) F.Matsuda, etal: NRIM, Vol. 11(1969), p. 43.
4) H.Nakagawa, etal: Trans. Japan Weld. Soc., Vol. 1(1970), p. 164.
5) M.Kato, etal: Trans. Japan Weld. Soc., Vol. 3(1972), p. 69.
6) For example, J.C.Borland: Brit. Weld. J., Vol. 7(1960), p. 508.
7) Yu.A.Sterenbogen, etal: Avt. Svarka, 1976, No. 11, p. 1.
8) Yu.A.Sterenbogen, etal: Avt. Svarka, 1969, No. 1, p. 5.
9) B.A.Movchan, etal: Avt. Svarka, 1969, No. 4, p. 6.
10) B.A.Movchan, etal: Avt. Svarka, 1968, No. 12, p. 4.
11) M.A.Abralov, etal: Svar. Proiz., 1978, No. 5, p. 1.
12) V.P.Chernysh, etal: Avt. Svarka, 1979, No. 3, p. 5.
13) F.Matsuda, etal: Trans. JWRI, Vol. 8(1979), p. 105.
14) Y.Arata, etal: Trans. JWRI, Vol. 5(1976), p. 135.
15) T.Senda, etal: Trans. Japan Weld. Soc., Vol. 2(1971), No. 2, p.1.
16) F.Matsuda: Unpublished.
17) F.Matsuda, etal: Trans. JWRI, Vol. 7(1978), p. 59.
18) Y.Arata, etal: Trans. JWRI, Vol. 5(1976), p. 153
19) H.D.Brody, etal: Trans. Met. Soc. AIME, Vol. 236(1966), p. 615.
20) H.Nakagawa, etal: Trans. Japan Weld. Soc., Vol. 5(1975), p. 192.
21) V.G.Revlin, etal: Int. Met. Rev., 1980, No. 1, p. 21.
22) M.Hansen: "Constitution of Binary Alloys", 2nd Edition, 1958, McGraw Hill.
23) W.Hume-Rothery, etal: J. Iron & Steel Inst., Vol. 202(1964), p. 534.
24) T.Okamoto, etal: Trans. ISIJ, Vol. 21(1981), p. 641.
25) T.Takahashi, etal: J. Japan Inst. Met., Vol. 43(1979), p. 1086 (in Japanese)
26) T.Takahashi, etal: J. Japan Inst. Met., Vol. 44(1980), p. 1089 (in Japanese)
27) D.B.Spencer, etal: Met. Trans., Vol. 3(1972), p. 1925.
28) T.Z.Kattamis: Trans. Met. Soc. AIME, Vol. 233(1965), p. 992.
29) J.C.Borland: Brit. Weld. J., Vol. 8(1961), p. 526.
30) W.R.Apblett, etal: Weld. J., Vol. 33(1954), 83s.
31) Japan Weld. Soc.: "Fractographic Atlas of Steel Weldments", 1982.
32) F.Matsuda, etal: Trans. JWRI, Vol. 6(1977), p. 81.
33) J.C.Borland: Weld. Met. Fab., 1979, March, p. 99.